Journal of Marine Science and Technology

Volume 23 | Issue 5 Article 4

DISCUSSION ON THE MAXIMUM STORM RADIUS EQUATIONS WHEN CALCULATING TYPHOON WAVES

Chun-Ming Chang
MIKE-HYDRO Tech. Ltd. Co., Taichung City, Taiwan, R.O.C.

Hui-Ming Fang
Department of Harbor and River Engineering, National Taiwan Ocean University, Keelung, Taiwan, R.O.C.,
d88520005@mail.ntou.edu.tw

Yung-Wei Chen
Department of Marine Engineering, National Taiwan Ocean University, Keelung, Taiwan, R.O.C.

Shih-Hsuan Chuang
MIKE-HYDRO Tech. Ltd. Co., Taichung City, Taiwan, R.O.C.

Recommended Citation

Chang, Chun-Ming; Fang, Hui-Ming; Chen, Yung-Wei; and Chuang, Shih-Hsuan (2015) "DISCUSSION ON THE MAXIMUM STORM RADIUS EQUATIONS WHEN CALCULATING TYPHOON WAVES," *Journal of Marine Science and Technology*: Vol. 23: Iss. 5, Article 4.
DOI: 10.6119/JMST-015-0226-1
Available at: https://jmstt.ntou.edu.tw/journal/vol23/iss5/4

Journal of Marine Science and Technology, Vol. 23, No. 5, pp. 608-619 (2015)
DOI: 10.6119/JMST-015-0226-1

DISCUSSION ON THE MAXIMUM STORM RADIUS EQUATIONS WHEN CALCULATING TYPHOON WAVES

Chun-Ming Chang[1], Hui-Ming Fang[2], Yung-Wei Chen[3], and Shih-Hsuan Chuang[1]

Key words: maximum wind speed radius, ECMWF, MIKE21 Spectral Wave model, typhoon waves.

ABSTRACT

In this paper, we conducted a series of numerical experiments to find the most suitable maximum wind speed radii for the parameterized typhoon model. Different maximum wind speed radius equations were used to generate different wind fields, which were then input into the MIKE21 Spectral Wave (SW) model. The wave height results from the MIKE21 SW model were compared with the measured results, and root-mean-square error (RMSE) analysis was conducted to find a good maximum wind speed radius equation for use as the basis for wind field generation in the future. The RMSEs were then scored according to this order. The lowest score indicated the best choice for the maximum wind speed radius equation. The SG02 equation (Silva et al., 2002) is the best maximum wind speed radius equation, was followed by the WA78 equation (Wang, 1978), it means that the radius of maximum wind is set to be 10% of the radius of Beaufort Scale 7 wind. For convenience of calculation, we recommend the WA78 equation, which is a reliable maximum wind speed radius equation.

I. INTRODUCTION

Taiwan is located in the west Pacific and has a subtropical climate. Every year from April to September, Taiwan is often afflicted by typhoons. According to the statistics from the Central Weather Bureau (Taiwan), a total of 1,872 typhoons from 1958 to April 2014 intruded on Taiwan or passed through the sea areas close to Taiwan; these typhoons significantly damaged the fishery facilities and the coastal engineering facilities in the Taiwan sea area. From the perspective of engineering design, typhoons are extreme conditions. It is necessary to design coastal facilities based on extreme conditions to withstand the extreme marine meteorological activities when typhoons intrude. However, coastal engineering design in Taiwan in the past has been determined by the wave conditions. Regression of the measured wave data (Liu et al., 2006) or wave estimation was often used (Liang et al., 2010). With the development of computers, the method of estimating waves in terms of spectra has also been applied to the estimation of coastal wind waves using numerical models. In wave spectrum numerical modeling, the wave energy equilibrium equation is often used as the governing equation. Third-generation spectral wave model has already been developed.

In the 1960s, Pierson and Moskowitz (1964) published the famous Pierson-Moskowitz (PM) spectrum, using spectra to express wind propagation and wave growth, which brought about the first-generation spectral wave model. The first-generation models were linear models, in which each component wave of the spectrum was treated as an individual wave that propagates independently, and there was no non-linear interaction between component waves. Later, with the success of the Joint North Sea Wave Project (Hasselmann et al., 1973), a number of non-linear wave behaviors were discovered that could not be explained using the PM spectrum-based first-generation spectral wave model. Therefore, the wave-wave interaction mechanism was introduced into the second-generation spectral wave model. According to the Sea Wave Modelling Project group (Allender et al., 1985), the second-generation spectral wave model could be generally classified into coupled hybrid models and coupled discrete models.

The third-generation spectral wave models were proposed in the 1980s. The Wave Model Development and Implementation Group (WAMDI, 1988) proposed a third-generation spectral wave model, WAM, in which a two-dimensional spectral transport equation was used as the governing equation; in addition, the equation included a growth term for wind generating waves as well as bottom friction, whitecapping, and wave-wave nonlinear dissipation terms. Hasselmann and

Paper submitted 07/08/14; revised 02/07/15; accepted 02/26/15. Author for correspondence: Hui-Ming Fang (e-mail: d88520005@mail.ntou.edu.tw).
[1] MIKE-HYDRO Tech. Ltd. Co., Taichung City, Taiwan, R.O.C.
[2] Department of Harbor and River Engineering, National Taiwan Ocean University, Keelung, Taiwan, R.O.C.
[3] Department of Marine Engineering, National Taiwan Ocean University, Keelung, Taiwan, R.O.C.

Hasselmann (1985) proposed discrete interaction approximations (DIA), which facilitated the otherwise difficult calculation of nonlinear wave-wave interactions.

The Simulating Waves Nearshore (SWAN) wave model (Booij et al., 1999) is an open source third-generation spectral wave model developed at the Delft University of Technology. The SWAN model was initially developed to calculate the growth and dissipation of wind waves in coastal regions; the fully implicit finite difference method is used as the discrete time method. The SWAN model is unconditionally stable with good calculation efficiency and has been widely used in the simulation of wind wave growth and dissipation (Ou et al., 1999; Liau et al., 2002; Ou et al., 2002).

The MIKE21 Spectral Wave model (SW) (Sørensen, Kofoed-hansen et al., 2004) is also a third-generation spectral wave model. This model has unstructured grid architecture and considers such mechanisms as wind wave generation, nonlinear wave-wave interaction, whitecapping dissipation, bottom friction, breaking effect, shoaling, and reflection; in addition, a cell-centered finite volume method is used to solve the wave action conservation equation.

Spectral wave model are essentially first-order partial differential equations. The equations represent the basic patterns of the wave propagation processes, while the non-homogeneous terms represent the physical processes or external forces that affect the waves. The boundary conditions and the initial conditions represent the surrounding environment and the initial state of simulation of the wave computational domain. In third-generation spectral wave model, among the source terms on the left side of the governing equation, the wave-generating wind power input is the most important production term, while the others are all dissipation terms. Therefore, the accuracy of wind field data significantly affects the numerical simulation results, especially the simulation of the waves in shallow water areas, in which the wind shear stress on the water surface is the main stress for wind generation, and thus the accuracy of the wind field data is extremely important.

There are many choices of wind field data sources for numerical simulation. For instance, NetCDF is available for downloading at certain international organizations, such as the European Center for Medium-Range Weather Forecasts (ECMWF) and the National Center for Atmospheric Research. However, for typhoon simulation, NetCDF presents certain disadvantages – overly poor temporal and spatial resolution. Generally speaking, the wind fields downloaded from ECMWF can be used as wind field input conditions for monsoon waves. However, for typhoon waves, the resolution of the wind fields downloaded from ECMWF is too poor to effectively describe the spiral variation of typhoon wind fields; therefore, typhoon wind fields are often simulated with multi-parameter typhoon models. Parameterized typhoon models are a type of mathematical model used to generate typhoons through a pressure gradient, and use a number of typhoon-related physical quantities, such as central pressure, storm radium, latitude, Coriolis force, maximum wind speed, and peripheral pressure, as model parameters. Typhoon model parameters can be obtained from certain meteorology websites, such as the Central Weather Bureau (Taiwan) or Japan Meteorological Agency. However, only storm radii of force 7 wind and force 10 wind are generally published, and the maximum wind speed radii are unknown. The maximum wind speed radius is the most important parameter for typhoon models.

Therefore, the objective of this study is to discuss how to use the aforementioned typhoon data to generate accurate wind fields through the typhoon model introduced below. The primary focus of this study is how to determine the maximum wind speed radius. Different maximum wind speed radius equations were used to generate different wind fields, which were then input into the MIKE21 SW model. The wave height results from the SW model were compared with the measured results, and root-mean-square error analysis was conducted to find a good maximum wind speed radius equation for use as the basis for wind field generation in the future.

II. MIKE21 SW NUMERICAL MODEL

The governing equation of the MIKE21 SW model is a wave action conservation equation:

$$\frac{\partial N}{\partial t} + \nabla \cdot \left(\vec{v} N \right) = \frac{S}{\sigma} \tag{1}$$

where $N(\vec{x}, \sigma, \theta, t) = E(\sigma, \theta)/\sigma$, and $E(\sigma, \theta)$ represents the energy density. $N(\vec{x}, \sigma, \theta, t)$ is the wave action density function, where t represents time; $\vec{x} = (x, y)$ is the Cartesian coordinate system; $\vec{v} = (C_x, C_y, C_\sigma, C_\theta)$ represent the components of the wind speed; S represents the source term; and σ represents the relative angular frequency, which should satisfy the following dispersion relation under wave-current interaction:

$$\sigma = \sqrt{gk \tanh\left(kd\right)} = \omega - \vec{k} \cdot \vec{U} \tag{2}$$

where g represents the acceleration of gravity; k represents the wave number; and $\vec{U}$ represents the current speed. The source term, S, is

$$S = S_{in} + S_{nl} + S_{ds} + S_{bot} + S_{surf} \tag{3}$$

where S_{in} represents the energy input by the wind force; S_{nl} represents the energy transfer of the wave-wave nonlinear interaction; S_{ds} represents the wave energy loss generated by whitecapping; S_{bot} represents the wave energy loss generated by bottom friction; and S_{surf} represents the wave energy loss generated by breaking waves. The group wave speed of the wave-current interaction can be expressed by

$$C_g = \frac{\partial \sigma}{\partial k} = \frac{1}{2}\left(1 + \frac{2kd}{\sinh(2kd)}\right)\frac{\sigma}{k} \quad (4)$$

The wind speed friction drive is the energy input by the wind force, expressed by the following equation:

$$s_{in}(f, \theta) = \gamma E(f, \theta) \quad (5)$$

where γ represents the wave growth rate. The wave energy dissipation induced by whitecapping dissipation is mainly caused by pressure. Therefore, the source function of the dissipation term is expressed by

$$S_{ds} \approx -\omega E \quad (6)$$

where ω represents the wave frequency, and E represents the wave energy density function. The energy loss rate caused by bottom friction can be expressed by

$$S_{bot}(f, \theta) = -\left(C_f + f_c(\bar{u} \cdot \bar{k})/k\right)\frac{k}{\sinh 2kd} E(f, \theta) \quad (7)$$

where C_f represents the friction coefficient; d represents the water depth; f_c represents the friction coefficient due to the current; $\bar{u}$ represents the current speed; and C_f generally ranges from 0.001 m/s to 0.01 m/s, but the actual value of C_f should be determined according to the actual bottom and ocean current conditions; if ocean currents are not considered, then $C_f = 0$.

When waves propagate to coastal areas, there will be a wave breaking effect due to the decreased water depth. In our model, this breaking effect is taken into consideration. The source function of the energy loss generated due to the wave breaking effect is as follows:

$$S_{surf}(f, \theta) = -\frac{2\alpha_{BJ} Q_b \bar{f}}{X} E(f, \theta) \quad (8)$$

where $\alpha_{BJ} \approx 1.0$ represents a parameter that needs to be verified; Q_b represents a relative parameter for breaking waves; $\bar{f}$ represents the mean frequency of waves; and X represents the ratio of the total wave energy to the maximum wave height, which can be expressed by

$$X = \frac{E_{tot}}{(H_m^2/8)} = \left(\frac{H_{rms}}{H_m}\right)^2 \quad (9)$$

where E_{tot} represents the total wave energy; H_m represents the maximum wave height; and $H_{rms} = \sqrt{8E_{tot}}$. When the water depth in the shallow water area is d, the maximum wave height can be expressed by $H_m = \gamma d$, where γ represents the breaking wave parameter, which ranges from 0.5 to 1.0, depending on the slope of the terrain. In our calculation, the variables α_{BJ} and γ were adjusted to 1.0 and 0.55, respectively. For random waves distributed based on Rayleigh wave height statistics, their relative parameter for breaking waves, Q_b, can be calculated using the following equation:

$$\frac{Q_b - 1}{\ln Q_b} = X = \left(\frac{H_{rms}}{H_m}\right)^2 \Leftrightarrow Q_b = \exp\left(\frac{-(1 - Q_b)}{(H_{rms}/H_m)^2}\right) \quad (10)$$

The finite volume method (FVM) is used to solve the MIKE21 SW model.

$$\frac{\partial}{\partial t}\int_{\Delta\theta_m}\int_{\Delta\sigma_l}\int_{A_i} N\, d\Omega\, d\sigma\, d\theta - \int_{\Delta\theta_m}\int_{\Delta\sigma_l}\int_{A_i}\frac{S}{\sigma} d\Omega\, d\sigma\, d\theta = \int_{\Delta\theta_m}\int_{\Delta\sigma_l}\int_{A_i} \nabla\cdot(\vec{F}) d\Omega\, d\sigma\, d\theta \quad (11)$$

where $\vec{F} = \left(F_x, F_y, F_\sigma, F_\theta\right) = \vec{v}N$ is the integral variable of Ω within A_i.

$$\frac{\partial N_{i,l,m}}{\partial t} = -\frac{1}{A_i}\left[\sum_{p=1}^{NE}(F_n)_{p,l,m}\Delta l_p\right] - \frac{1}{\Delta\sigma_l}\left[(F_\sigma)_{i,l+1/2,m} - (F_\sigma)_{i,l-1/2,m}\right] - \frac{1}{\Delta\theta_m}\left[(F_\sigma)_{i,l,m+1/2} - (F_\sigma)_{i,l,m-1/2}\right] + \frac{S_{i,l,m}}{\sigma_l} \quad (12)$$

where $\theta_m = (m - 1)\Delta\theta$, $\Delta\theta_m = 2\pi/N_\theta$, $m = 1 \sim N_\theta$, and N_θ represents the direction partition; $\Delta\sigma_l$ and $\Delta\theta_m$ represent the frequency and the angular space, respectively.

Time integration is based on the explicit Euler scheme,

$$N^*_{i,l,m} = N^n_{i,l,m} + \Delta t\left(\frac{\partial N_{i,l,m}}{\partial t}\right)^n,$$

where $\left(\frac{\partial N_{i,l,m}}{\partial t}\right)^n$ can be obtained from Eq. (12).

Owing to the explicit scheme being adopted, it must satisfy the stability condition:

$$C_{r_{i,l,m}} = \left|c_x\frac{\Delta t}{\Delta x_i}\right| + \left|c_y\frac{\Delta t}{\Delta y_i}\right| + \left|c_\sigma\frac{\Delta t}{\Delta\sigma_l}\right| + \left|c_\theta\frac{\Delta t}{\Delta\theta_m}\right| < 1 \quad (13)$$

III. TYPHOON WIND FIELDMODELS

The common typhoon wind field models are summarized below:

- Jelesnianski's axisymmetric typhoon model (1965)

  The wind velocity $V_g(r)$ on a point at a distance r from the

typhoon center is expressed as follows

$$\begin{cases} V_g(r) = V_{\max}\left(\dfrac{r}{R_{mw}}\right)^{3/2}\dfrac{1}{r}\left[Ai + Bj\right], & 0 < r < R_{mw} \\ V_g(r) = V_{\max}\left(\dfrac{r}{R_{mw}}\right)^{-1/2}\dfrac{1}{r}\left[Ai + Bj\right], & r \geq R_{mw} \end{cases} \tag{14}$$

where $V_{\max}$ is the maximum wind in a distance r from its center. i and j are unit vectors in x and y directions respectively. Furthermore, $A = -(y\cos\phi + x\sin\phi)$, $B = x\cos\phi - y\sin\phi$, where ϕ is the ingress angle, with which the wind is directed across the isobars into the interior of a typhoon.

The moving wind field is expressed by the following equation:

$$\begin{cases} V_g(r) = V_{\max}\left(\dfrac{r}{R_{mw}}\right)^{3/2}\dfrac{1}{r}\left[Ai + Bj\right] + \\ \dfrac{r}{R_{mw} + r}\left[U_0 i + V_0 j\right], & 0 < r < R_{mw} \\ V_g(r) = V_{\max}\left(\dfrac{r}{R_{mw}}\right)^{-1/2}\dfrac{1}{r}\left[Ai + Bj\right] + \\ \dfrac{r}{R_{mw} + r}\left[U_0 i + V_0 j\right], & r \geq R_{mw} \end{cases} \tag{15}$$

where U_0 and V_0 are x and y components of the moving velocity of typhoon center, respectively.

The pressure field $p(r)$ is expressed by the following equation:

$$\begin{cases} p(r) = \dfrac{\rho_a}{3}\left(\dfrac{V_{\max}}{\gamma_0}\right)^2\left(\dfrac{r}{R_{mw}}\right)^3 + p_c, & 0 < r < R_{mw} \\ p(r) = \rho_a\left(\dfrac{V_{\max}}{\gamma_0}\right)^2\dfrac{R_{mw}}{r} + p_c, & r \geq R_{mw} \end{cases} \tag{16}$$

- Young and Sobey 1981

Young and Sobey (1981) proposed the wind velocity $V_g(r)$ can be expressed as follows

$$\begin{cases} V_g(r) = V_{\max}\left(\dfrac{r}{R_{mw}}\right)^7 \exp\left(7\left(1 - \dfrac{r}{R_{mw}}\right)\right), & r < R_{mw} \\ V_g(r) = V_{\max}\exp\left(\left(0.0025R_{mw} + 0.05\right)\left(1 - \dfrac{r}{R_{mw}}\right)\right), & r \geq R_{mw} \end{cases} \tag{17}$$

In the above equation, $V_b(r)$ represents the distribution function of the outward wind gradient from the typhoon center along the storm radius; $p(r)$ represents the pressure field at radius:

$$p(r) = p_c + \left(p_n - p_c\right)\exp\left(-\frac{R_{mw}}{r}\right). \tag{18}$$

where p_c the central pressure, and p_n the ambient atmospheric pressure far from the storm.

- Holland (1980)

Following Holland (1980), the gradient wind can be expressed as

$$V_g(r) = \sqrt{\left(p_n - p_c\right)\frac{B}{\rho_A}\left(\frac{R_{mw}}{r}\right)^B \exp\left(-\frac{R_{mw}}{r}\right)^B + \left(\frac{r \cdot f}{2}\right)^2} - \frac{r \cdot |f|}{2} \tag{19}$$

$V_g(r)$ is the gradient wind at radius r from the center of the storm, f is the Coriolis parameter, ρ_A the air density. The maximum wind speed $V_{\max}$ at this radius can be estimated as

$$V_{\max} = \sqrt{\left(p_n - p_c\right)\frac{B \cdot e}{\rho_A}} \tag{20}$$

The dimensionless parameter B defines the shape of the wind field with increasing distance from the center of the hurricane. Holland (1980) has shown that B can be related to the central pressure p_c. A linear fit to his data yields

$$B = 2 - (p_c - 900)/160 \tag{21}$$

The pressure field $p(r)$ can be expressed with the dimensionless parameter B by the following equation

$$p(r) = p_c + \left(p_n - p_c\right)\exp\left(-\frac{R_{mw}}{r}\right)^B \tag{22}$$

where $1 < B < 2.5$.

In the MIKE21 SW model, the Holland (1980) typhoon model was adopted and V_{10} must be used as the input condition. To convert the aforementioned wind speed to V_{10}, a geostrophic wind correction must be performed:

$$V_{10} = K_m \cdot V_g(r) \tag{23}$$

The parameter K_m can be determined as following formula:

$$K_m = \begin{cases} 0.81, & V_g < 6\ m/s \\ 0.81 - 2.96 \cdot 10^{-3}(V_g - 6), & 6 < V_g < 19.5\ m/s \\ 0.77 - 4.31 \cdot 10^{-3}(V_g - 19.5), & 19.5 < V_g < 45\ m/s \\ 0.66, & V_g > 45\ m/s \end{cases} \tag{24}$$

Because the typhoon wind field will become asymmetrical during its propagation, a correction must be performed:

$$V_{10} = K_m \cdot V_g(r) + \delta_{fm} V_{fm} \cos(\theta_{\max} - \theta) \quad (25)$$

IV. DISCUSSION OF DIFFERENT MAXIMUM WIND SPEED RADII

Silva, Georges, Paulo, Gustavo, and Gabriel (2002) (SG02 et seq.) performed nonlinear regression on the 1,280 typhoons that occurred from 1949 to 2002 (739 in the Pacific and 541 in the Atlantic) and the meteorological data published every 6 hours from 1972 to 2001 (30 years in total) by the National Oceanic and Atmospheric Administration (NOAA), obtaining the following relation between pressure and maximum wind speed radius:

$$R_{mw} = 0.4785 p_c - 413 \text{ (km)} \quad (26)$$

where p_c represents the central pressure of the typhoon (mb).

Wang (1978) (WA78 et seq.) suggested that the maximum wind speed radius should be 1/10 of the force 7 storm radius.

$$R_{mw} = 0.1 R_7 \quad (27)$$

Ou et al. (1999) (OH99 et seq.) obtained the following regression equation based on the typhoon data from 1945 to 1997 published by the Central Weather Bureau (Taiwan):

$$R_{mw} = -1.529 \cdot 10^{-5} p_c^3 + 0.04036 p_c^2 - 35.645 p_c + 10608.8 \quad (28)$$

Hsu and Babin (2005) (HB05 et seq.) used satellite typhoon images to solve the relation between speed and maximum wind speed radius proposed by Anthes (1982), which is shown below:

$$V_r = V_{\max} \left(\frac{R_{mw}}{r} \right)^x \quad (29)$$

where x represents an undetermined coefficient that relies on measured data; generally, $x = 0.7$. Hsu and Babin (2005) used the buoy data of hurricane Lili to solve the above equation and compared the result with the satellite images and buoy locations; they discovered that R_{mw} matched the distance calculated from the satellite images very well.

$$R_{mw} = r \left(\frac{V_r}{V_{\max}} \right)^{\frac{1}{x}} \quad (30)$$

Graham and Nunn (1959) (GN59 et seq.) suggested the following empirical equation for maximum wind speed radius:

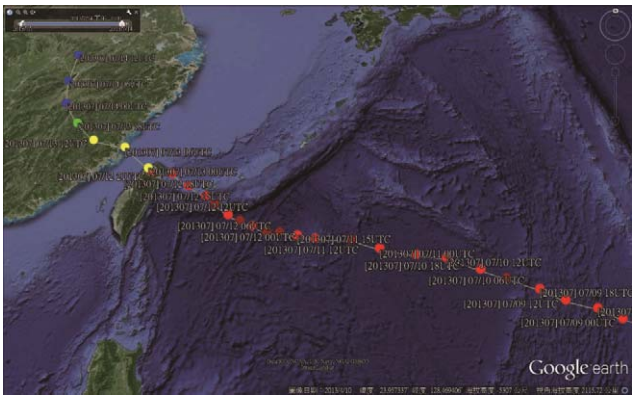

Fig. 1. Path of Typhoon Soulik.

$$R_{mw} = 28.52 \cdot \tanh\left[0.0873(\phi - 28)\right] + \frac{12.22}{\exp\left(\frac{1013 - p_c}{33.86}\right)} + 0.2 V_f + 37.22 \quad (31)$$

where V_f represents the advancing speed of the typhoon, and ϕ represents the latitude.

Willoughby and Rahn (2004) (WR04 et seq.)

$$R_{mw} = 51.6 \exp\left(-0.0223 V_{\max} + 0.0281 \phi\right) \quad (32)$$

In this study, Typhoon Soulik, which reached Taiwan in July 2013, was used as the study object, and the aforementioned numerical model was used. Fig. 1 shows the path of Typhoon Soulik. The hurricane was initially a tropical cyclone, which formed at 00 coordinated universal time (UTC) on July 7, 2013 at approximately (151.06E, 19.04N). The center of the typhoon was located in the sea area around the Guishan Island at 18 UTC on July 12, 2013. Typhoon Soulik made landfall in the Gongliao District, New Taipei City at 00 Taiwan Standard Time (TST) on July 13, 2013. Affected by the terrain, the path of the typhoon turned south. Typhoon Soulik passed to the ocean from Hsinchu County at 08 TST on July 13, 2013. When Typhoon Soulik was approaching Taiwan, the Central Weather Bureau issued a warning in which Typhoon Soulik was labeled as a severe typhoon, which significantly affected the sea area around Taiwan. Therefore, Typhoon Soulik is a representative typhoon.

First, the 6 aforementioned different maximum wind speed radii were calculated, and then the typhoon paths, the central pressure values, and the shape parameter, B were input into the DHI MIKE21 toolbox to generate the typhoon wind field and pressure field. Fig. 2 shows the typhoon wind field model of Typhoon Soulik. The red text is the time after 08 TST, July 7, 2013, while the white text marks the locations of buoys in the data. TD represents the buoys in the open sea near Taitung; GSD represents the Guishan Island buoys; HC represents the

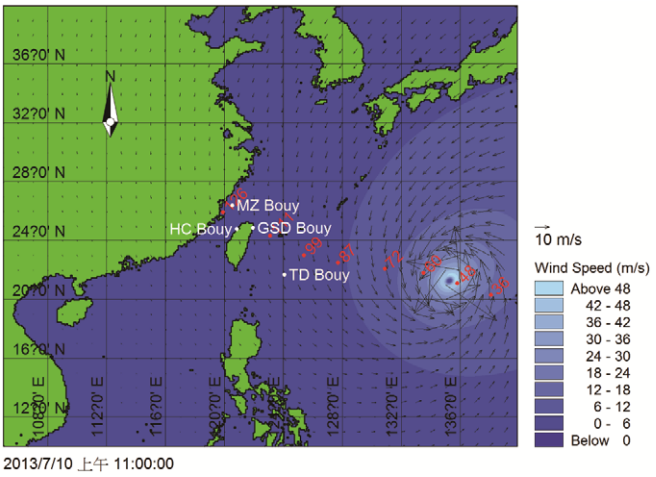

Fig. 2. Typhoon wind field of the Typhoon Soulik model by WA78.

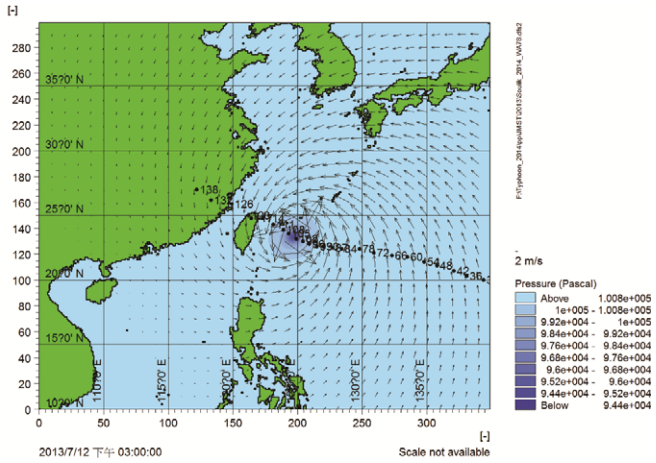

Fig. 3. Typhoon pressure field of the Typhoon Soulik model by WA78. Based on various equations.

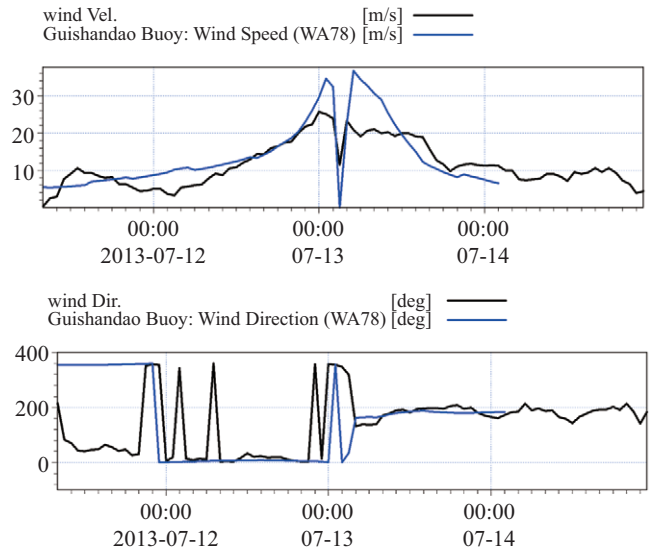

Fig. 4. Comparison between the wind data measured on the Guishan Island and the wind speed and wind direction of the typhoon model by WA78.

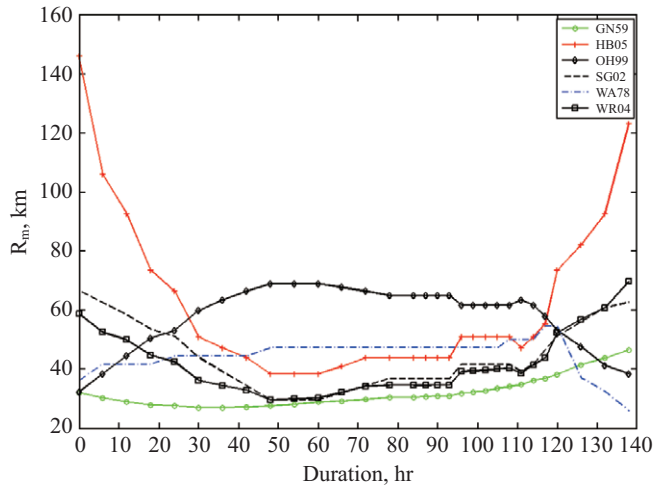

Fig. 5. Comparisons of the time variation of the radius of maximum wind.

Hsinchu buoys; MZ represents the Matsu buoys. Fig. 3 shows the planar distribution map of the pressure field of the Typhoon Soulik model. The pressure at the center of the typhoon was the lowest; the wind speed was higher the closer it was to the center of the typhoon; thus, the wind field of the typhoon model was preliminarily in agreement with the actual situation. In addition, to verify the reliability of the wind field generated by the model, the wind data measured at the Guishan Island station were compared with the wind generated by the typhoon model. Fig. 4 shows the comparison results. Both the wind speed and the wind direction generated by the typhoon model were in good agreement with the measured data.

Fig. 5 shows that the maximum wind speed radii of the aforementioned equations varied with time (the initial time is 00 UTC on July 8, 2013); thus, the variation trend of the maximum wind speed radius of the typhoon over time could be understood, and it could also be determined whether such a trend was reasonable. Fig. 5 clearly shows that the Typhoon Soulik existed 30 hours before the calculation of the typhoon model started. However, Fig. 5 shows that the maximum wind speed radii of the Typhoon Soulik calculated using the HB05, SG02, and WR04 equations were even greater than the maximum wind speed radius when the typhoon was formed; therefore, the results from these equations exhibited an overestimating trend. A similar situation occurred 120 hours later when the typhoon passed Taiwan. Overall, the maximum wind speed radius calculated using the GN59 equation was the smallest, while the maximum wind speed radius calculated using the OH99 equation was the largest. The maximum wind speed radius ranged from 10 km to 70 km during 30~120 hours after the calculation started, and the maximum wind speed radius was mainly concentrated in the range from 10 km to 40 km.

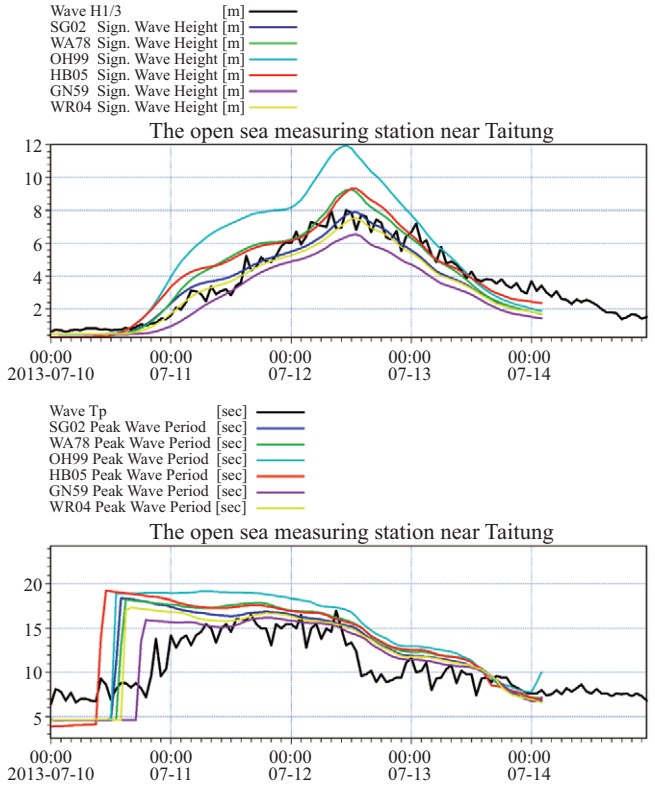

Fig. 6. Comparison between the wave height results calculated using the SW model and the measured results under different maximum storm radii (the open sea measuring station near Taitung).

V. RESULTS AND DISCUSSION

Fig. 6 compares the wave height data measured at the open sea buoy station near Taitung and the calculation results from the SW model, showing that the calculation results of the waves caused by the wind fields of the equations were generally the same. The wave height and the periodic value calculated using the SG02 equation were the best, while the calculation results from the OH99 equation deviated the most from the measured data. However, an interesting phenomenon occurred in the comparison among the maximum periods. There was a jump in every maximum period at approximately 1200 TST on July 10, 2012. To investigate the cause of this phenomenon, we plotted the full wave spectrum (frequency spectrum + direction spectrum) before and after 1200 TST on July 10, 2012 in Figs. 7 and 8 and compared them. Fig. 7 shows that at 0900 TST on July 10, 2013, the comprehensive results of wind waves and swell were such that the wave angle was northward, the maximum period was approximately 7 seconds, and swell were the main component. Fig. 8 shows the full wave spectrum at 1200 TST on July 10, 2013, and the location of the center of the typhoon at this moment is shown in Fig. 2. Fig. 8 shows that main values in 2 directions occurred during the maximum period – 7 seconds (north) and 18 seconds (east); in addition, swell were still the main component. Based on the above analysis of the full wave spectrum,

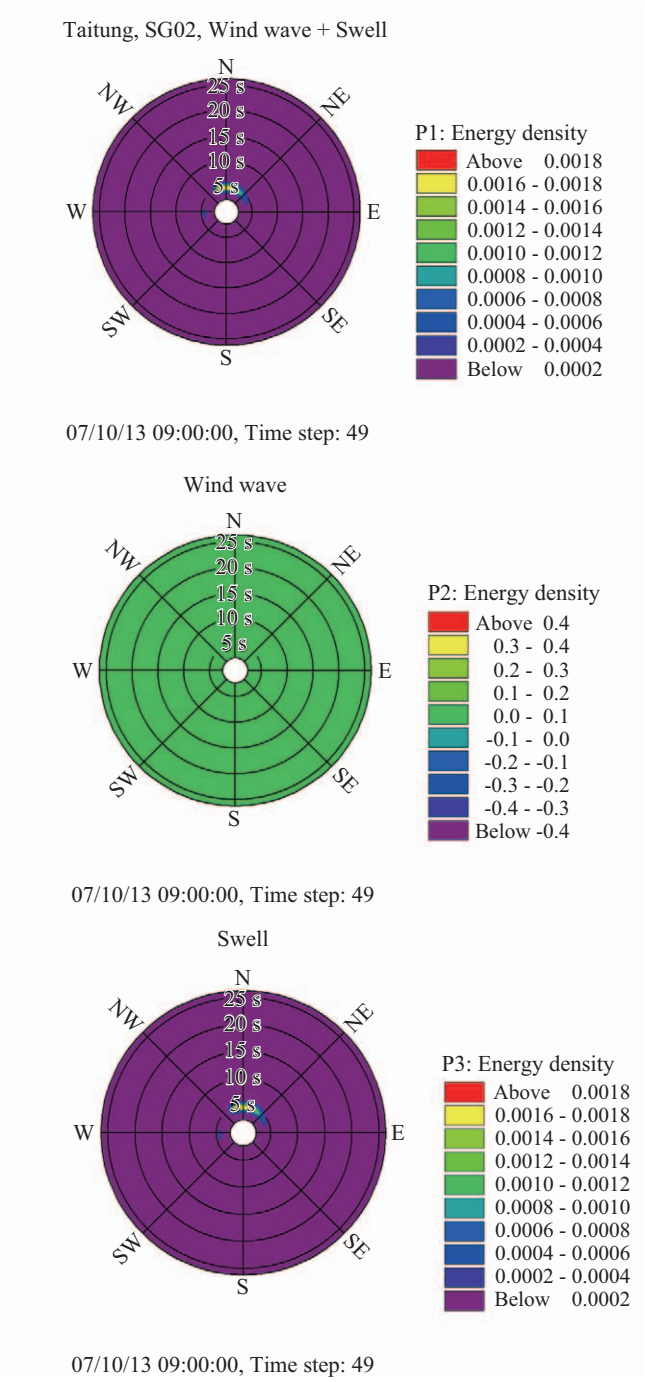

Fig. 7. Spectral analysis of the open sea buoy location near Taitung (SG02 calculation results-1).

we can clearly explain the jump phenomena in the maximum wave periods shown in Fig. 6, which also indicates that for the typhoon wind force data generated without the addition of the background wind field, no wind wave could be generated because there was no wind action at the locations far from the typhoon during the initial stage of calculation; therefore, it was impossible to use the maximum wave period of the wind waves as the background value. When the typhoon swell

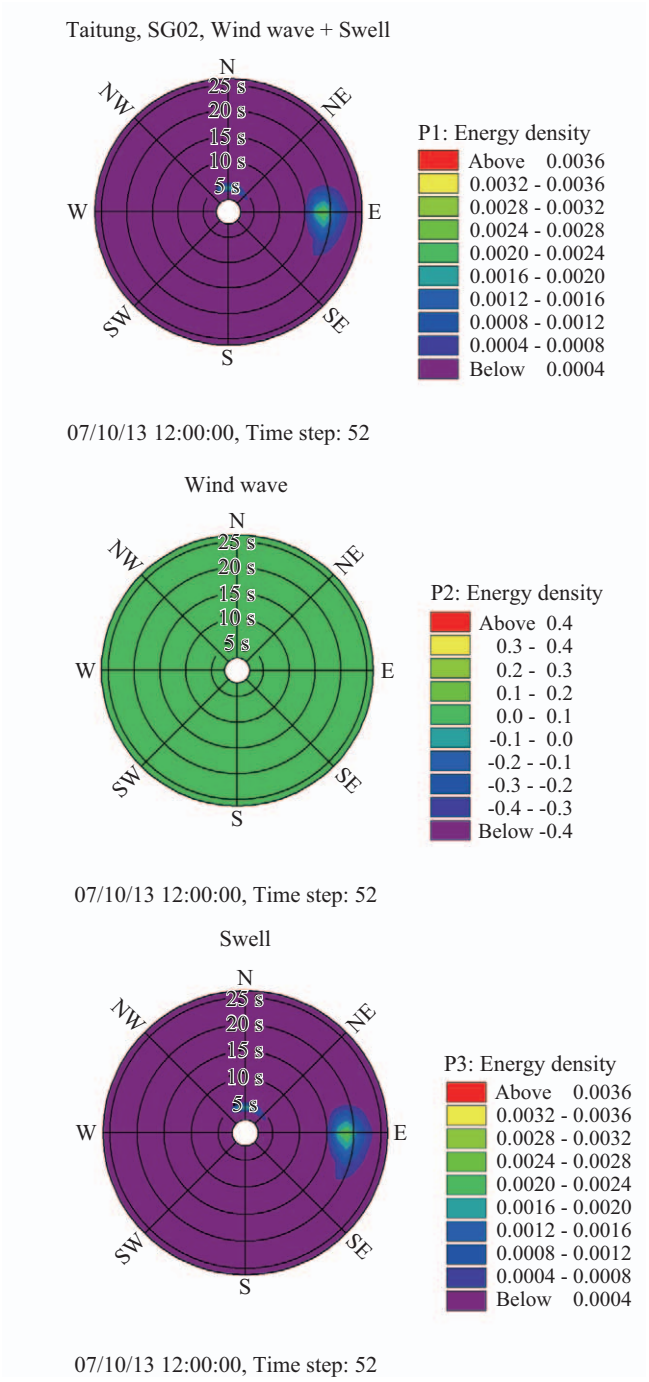

Fig. 8. Spectral analysis of the open sea buoy location near Taitung (SG02 calculation results-2).

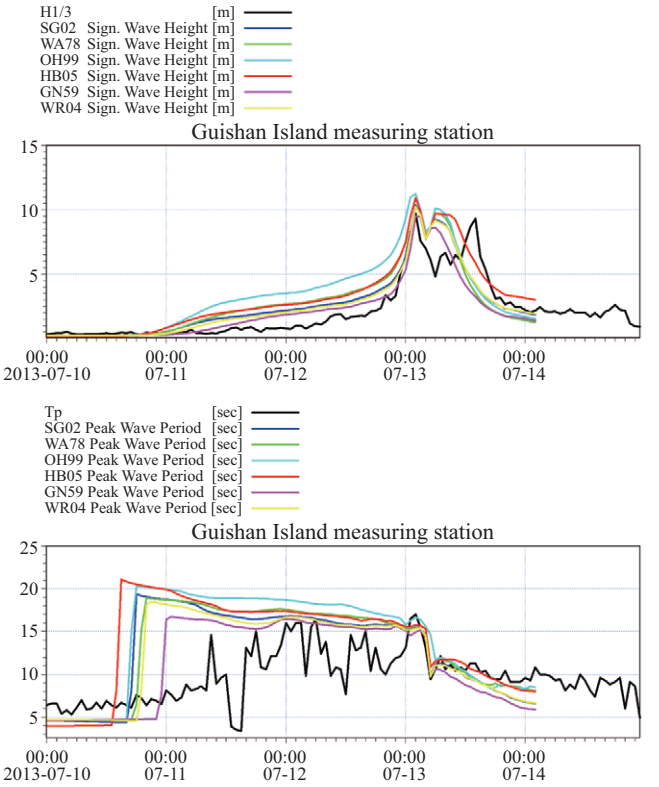

Fig. 9. Comparison of the wave height results calculated using the SW model and the measured results under different maximum storm radii (Guishan Island measuring station).

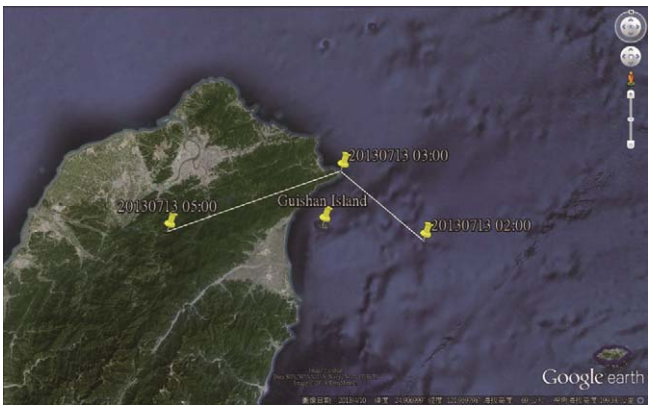

Fig. 10. Path of Typhoon Soulik near Guishan Island.

arrived from afar, a jump phenomenon in the maximum period immediately occurred.

Fig. 9 compares the calculation results from different maximum wind speed radius equations and the wave data measured at the Guishan Island. The figure shows the wave heights calculated using different maximum wind speed radius equations; the first peaks were very close to the peak of the measured wave height, while the second peaks all occurred relatively earlier because the typhoon model could not reflect the actual topographic effect. The Guishan Island Measuring Station was located in the sea area between Taiwan Island and Guishan Island; therefore, when the typhoon reached the area near Guishan Island, the wind domain and wind duration both enabled the wave height to grow to its first peak. Fig. 10 shows that after Typhoon Soulik landed at Cape San Diego on Taiwan Island at 03:00 TST on July 13, 2013, the actual wind power decreased due to the topographical effect (Fig. 4). However, the typhoon model could not reflect the effect of

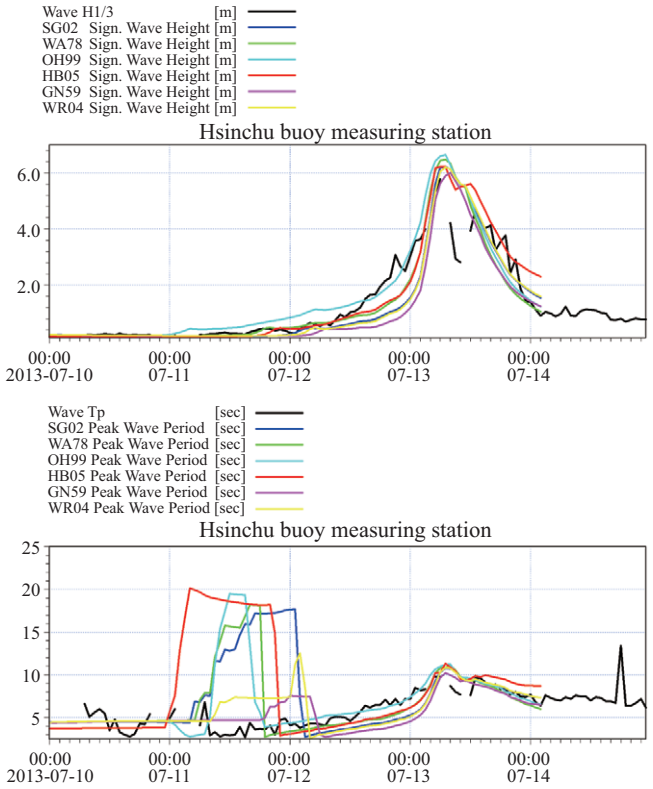

Fig. 11. Comparison of the wave height results calculated using the SW model and the measured results under different maximum storm radii (Hsinchu buoy measuring station).

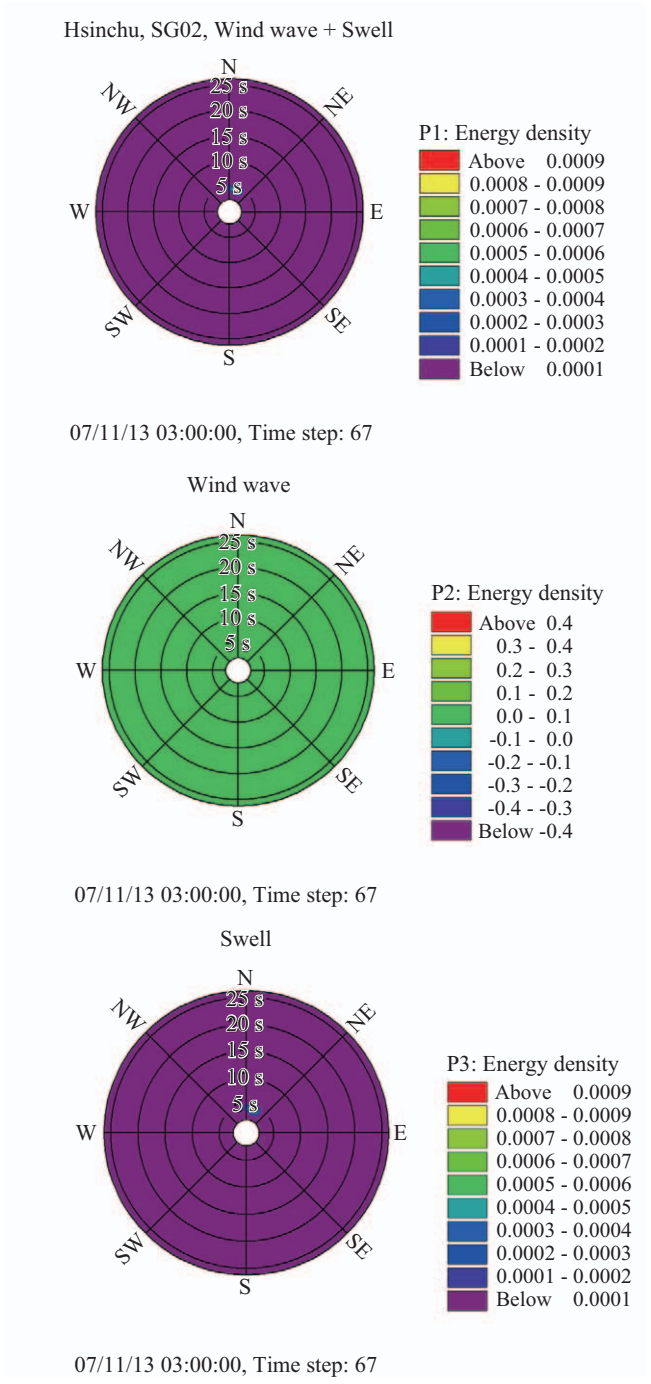

Fig. 12. Spectral analysis of the Hsinchu buoy location (SG02 calculation results-1).

the actual topography on wind power; therefore, as shown in Fig. 4, after Typhoon Soulik landed on Taiwan Island at 03:00 TST on July 13, 2013, the wind power gradually decreased (based on the measured data), while wind power peaks emerged in the WA78 typhoon model. This result is clearly not in agreement with the measured data; thus, a 2nd peak occurred not long after the 1st peak in all the results calculated using the equations.

Fig. 11 compares the calculation results of different maximum wind speed radii and the data measured at the Hsinchu buoy measuring station, showing that the calculation results of different maximum wind speed radii all showed a similar trend to the measured wave heights; in addition, there was no significant difference between the calculation results for different maximum wind speed radii and the measured data in terms of wave height peaks. The comparison of the maximum wave periods also shows a jump phenomenon. The difference from the previous case is that in the previous case, the maximum wave periods gradually approached the measured value after the single jump, while in this case, there was another sudden jump 1 day after the first (at 00:00 TST on July 12, 2013), after which the maximum wave periods gradually approached the measured value. We now analyze the cause. Fig. 12 shows that northeastward swell emerged at 03:00 TST on July 11, 2013, and the maximum wave period was approximately 7 seconds. Fig. 13 shows that a northwestward swell component emerged at 12:00 TST on July 11, 2013, and the maximum wave period was approximately 17 seconds. It is worth noting that no wind wave component is present in the 2 aforementioned figures. Fig. 14 shows that a northward wind wave component emerged, and the maximum wave period was approximately 3 seconds. The top figure in Fig. 14 shows the combination of the swell and the wind waves; within 7 seconds, the northward wave component was more intense than

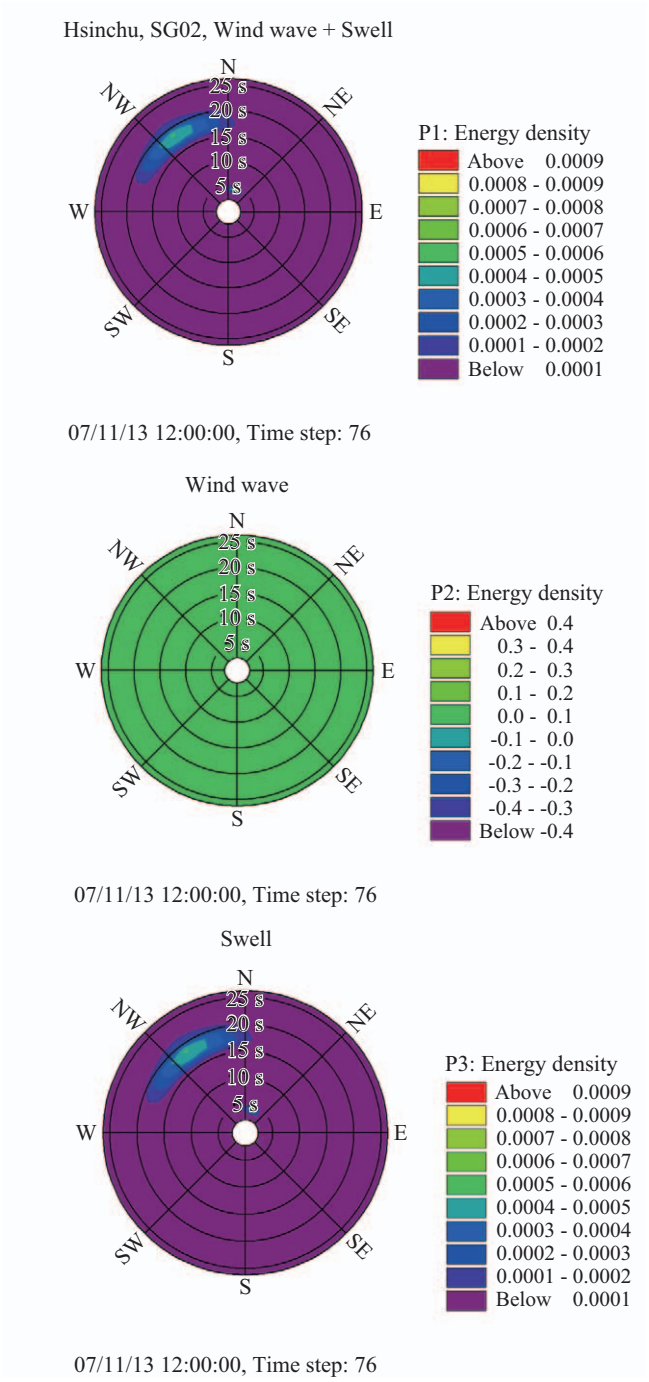

Fig. 13. Spectral analysis of the Hsinchu buoy location (SG02 calculation results-2).

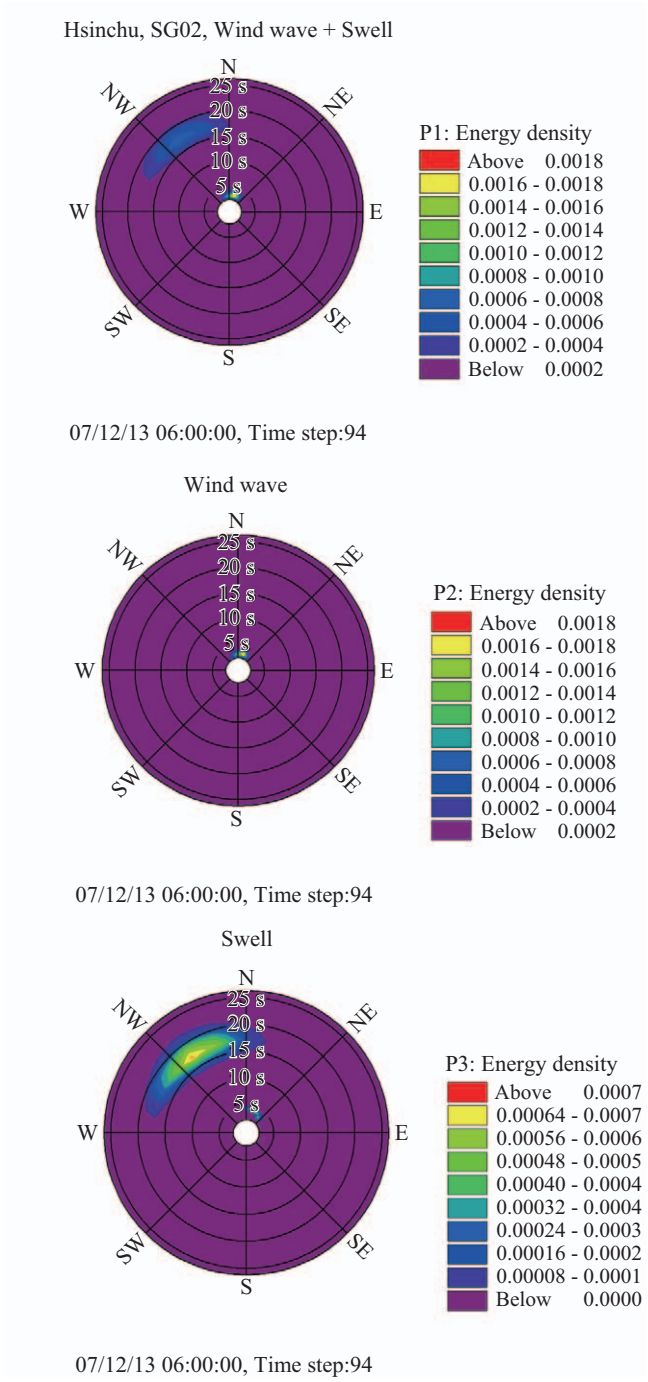

Fig. 14. Spectral analysis of the Hsinchu buoy location (SG02 calculation results-3).

the northwestward surge component, and thus, the northward components predominated.

Fig. 15 compares the calculation results of different maximum wind speed radii and the data measured at the Matsu buoy measuring station. The simulation results of wave heights using different equations were generally close to the measured wave height. There was also a jump in each calculated maximum wave period; the cause of this phenomenon might be the same as the observation at the open sea buoys near Taitung.

To compare the calculation results of the wave heights of the typhoon models generated by different maximum wind speed radii, we performed root-mean-square error (RMSE) analysis on the above calculation results and sorted the results in ascending order according to their RMSEs. The RMSEs were then scored according to this order. The lowest score indicated the best choice for the maximum wind speed radius

Table 1. Calculation results and analysis of RMSEs.

Eq.	RMSE_TD		RMSE_GSD		RMSE_HC		RMSE_MZ		total points
SG02	0.44	1	3.02	2	0.48	4	0.6	2	9
WA78	0.71	3	3.07	3	0.41	3	0.81	1	10
OH99	3.75	6	3.41	5	0.36	1	1.3	6	18
HB05	0.75	4	3.7	6	0.37	2	0.74	3	15
GN59	0.98	5	2.86	1	0.63	6	0.94	5	17
WR04	0.46	2	3.08	4	0.5	5	0.57	1	12

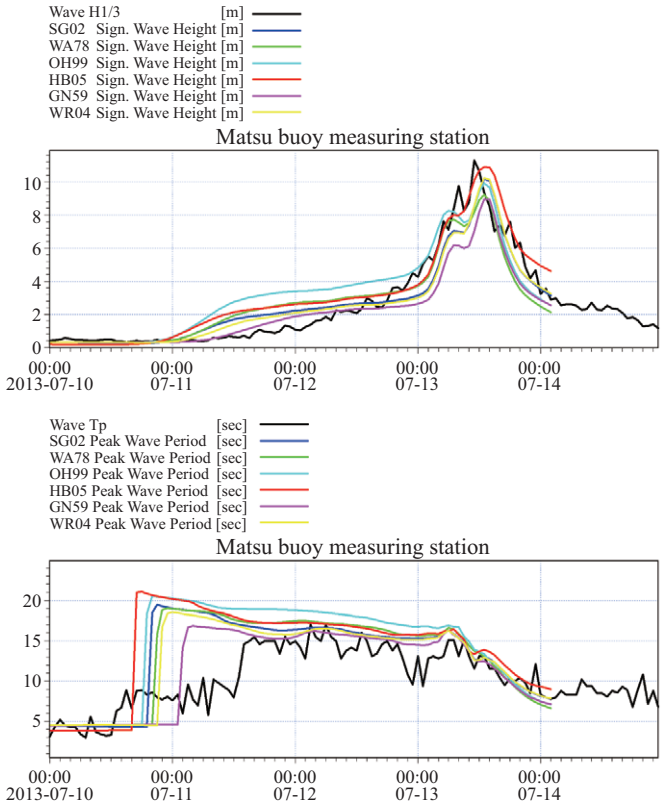

Fig. 15. Comparison of the wave height results calculated using the SW model and the measured results under different maximum storm radii (Matsu buoy measuring station).

equation. Table 1 lists the results. The analysis results show that the best maximum wind speed radius equation was the SG02 equation, followed by the WA78 equation.

VI. CONCLUSIONS

In this study, 6 commonly used maximum wind speed radius equations were used to generate the wind field of a typhoon model, which was then used as the source term for wave generation in wind wave calculation using the SW model. To verify the reliability of wind field generation by the typhoon model, the wind data measured on the Guishan Island were compared with the results of the typhoon model; the comparison shows that the two were in agreement.

To find the best maximum wind speed radius equation, we compared the wave heights from six different equations, including stations in the open sea near Taitung, the Guishan Island, Hsinchu and Matsu, with those of field data, and we also calculated the RMSEs were calculated. Finally, the RMSEs of all the measuring stations were scored according to their sorting order. The SG02 equation was the best, followed by the WA78 equation. For convenience of calculation, we recommend the WA78 equation, which is a reliable maximum wind speed radius equation.

REFERENCES

Allender, J. H., T. P. Barnett, L. Bertotti, J. Bruinsma, V. J. Cardone, L. Cavaleri and W. J. P. D. Voog (1985). Sea wave modeling project (SWAMP). An intercomparison study of wind wave predictions models, part 1: Principal results and conclusions. Ocean Wave Modeling, 3-153.

Anthes, R. A. (1982). Tropical Cyclones: Their Evolution, Structure and Effects. Amer Meteorological Society.

Booij, N., R. C. Ris and L. H. Holthuijsen (1999). A third-generation wave model for coastal regions: 1. Model description and validation. Journal of Geophysical Research 104, 7649-7666.

Graham, H. E. and D. E. Nunn (1959). Meteorological considerations pertinent to standard project hurricane, Atlantic and Gulf Coasts of the United States. National hurricane research project report No.74, Washington, D. C: U. S. Weather Bureau.

Group, T. W. (1988). The WAM Model–a third generation ocean wave prediction model. Journal of Physical Oceanography 18, 1775-1810.

Hasselmann, K., T. P. Barnett, T. P. Bouws, E. H. Carlson, D. E. Cartwright, K. Enke, J. A. Ewing, H. Gienapp, D. E. Hasselmann, P. Kruseman, A. Meerburg, A. Müller, P. D. J. Olbers, K. Richter, W. Sell and H. Walden (1973). Measurements of wind-wave growth and swell decay during the Joint North Sea Wave Project (JONSWAP), Dtsch. Hydrogr. Z. Suppl 12, 1-95.

Hasselmann, S. and K. Hasselmann (1985). Computations and parameterizations of the nonlinear energy transfer in a gravity-wave spectrum. Part I: A new method for efficient computations of the exact nonlinear transfer integral. Journal of Physical Oceanography 15, 1369-1377.

Holland, G. J. (1980). An analytic model of the wind and pressure profiles in hurricanes. Monthly Weather Review 108, 1212-1218.

Hsu, S. A. and A. Babin (2005). Estimating the radius of maximum wind via satellite during Hurricane Lili (2002) over the Gulf of Mexico. National Weather Association Electronic Journal.

Jelesnianski, C. P. (1965). A numerical calculation of storm tides induced by a tropical storm impinging on a continental shelf. Monthly Weather Review 93, 343-358.

Liang, N.-K., J.-J. Lin and H.-M. Tseng (2010). A study on typhoon swell forecasting scheme. Journal of Coastal and Ocean Engineering 10, 219-236. (in Chinese)

Liau, J.-M., S.-H. Ou, T.-W. Hsu, C.-C. Fang and S.-Y. Tzeng (2012). The characteristic of typhoon waves in Taiwan area by swan model. Proceedings of the 24th Ocean Engineering Conference in Taiwan, 469-476. (in Chinese)

Liou, J.-C., C.-S. Chang, J.-C. Hsu, L.-S. Ho and W.-Y. Lin (2006). A study on wave condition in Taipei harbor. Proceedings of the 28th Ocean Engineering Conference in Taiwan, 835-839. (in Chinese)

Ou, S.-H., T.-W. Hsu, S.-Y. Tzang, C.-C. Fang and J.-M. Liau (1999). The study of typhoon waves in Taiwan area by swan model. Proceedings of the 21th Ocean Engineering Conference in Taiwan, 87-95. (in Chinese)

Ou, S.-H., J.-M. Liau, T.-W. Hsu and S.-Y. Tzang (2002). Simulating typhoon waves by SWAN wave model in coastal waters of Taiwan. Ocean Engineering 29, 947-971.

Pierson, W. J. and L. Moskowitz (1964). A proposed spectral form for fully

developed wind seas based on the similarity theory of S. A. Kitaigorodskii. Journal of Geophysical Research 69, 5181-5190.

Silva, R., G. Georges, S. Paulo, B. Gustavo and B. G. D. Gabriel (2002). Oceanographic vulnerability to hurricanes on the Mexican coast. Proceedings of 28th Conference on Coastal Engineering, 39-51.

Sørensen, O. R., H. Kofoed-hansen, M. Rugbjerg and L. S. Sørensen (2004). A third-generation spectral wave model using an unstructured finite volume technique. Proceedings of 29th Conference on Coastal Engineering, 19-24.

Wang, G. C. Y. (1978). Sea-level pressure profile and gusts within a typhoon circulation. Monthly Weather Review 106, 954-960.

Willoughby, H. E. and M. E. Rahn (2004). Parametric representation of the primary hurricane vortex. Part I: observations and evaluation of the holland (1980) model. Monthly Weather Review 132, 3033-3048.